TRAJECTORY CONTROL OF A THREE DOF DUAL ARM SPACE ROBOT WITH SMALL ATTITUDE DISTURBANCE

Haresh Patolia[(a)], P. M. Pathak[(b)], S. C. Jain[(c)]

[(a)] [(b)] Robotics and Control Laboratory, Mechanical and Industrial Engineering Department,
Indian Institute of Technology, Roorkee, India, 247667
[(c)] Mangalayatan University, Aligarth, India

[(a)] haresh_patolia@yahoo.co.in, [(b)] pushpfme@iitr.ernet.in, [(c)]sjainfme@yahoo.com

ABSTRACT
This work presents a trajectory planning strategy for a three degree of freedom (DOF) dual arm space robot in work space. The strategy is based on the principle of dynamic coupling between the tip motion and the vehicle motion of the space robot. The strategy uses the two arms of three link serial manipulator. One arm called mission arm achieves the trajectory control task while the other arm called balance arm moves in a way to reduce the attitude of the vehicle. A robust overwhelming controller is used for trajectory control of tip of the mission arm. The first and second joint rotations of balance arm are based on the first and second joint rotations of mission arm whereas the third joint rotation of balance arm is carried out such that small attitude disturbance of vehicle takes place. An example of three DOF dual arm space robot is considered to illustrate the methodology. Bond graph has been adopted as modeling tool as it facilitates the system modeling from the physical paradigm itself and it is easy to develop various control strategies by modifying the physical paradigm.

Keywords: dual arm space robot, robust overwhelming controller, attitude control, bond graph modeling

1. INTRODUCTION

In a large number of space applications like maintenance of components, capture of floating objects, removal of debris or old satellites, orbital replacement unit operations, refueling etc., the manipulator motion is required to be controlled precisely. In a free-floating space robotic system, the spacecraft position and the attitude are not actively controlled using external jets or thrusters during manipulator activity. Due to the conserved linear and angular momenta, the spacecraft moves freely in response to the dynamic disturbances caused by the manipulator motion. Such disturbances may result in significant deviation of the end-effector from the desired trajectory, and are particularly significant when the manipulator is holding a heavy payload. Moreover, the angular momentum conservation constraints are non-integrable rendering the system non-holonomic. Hence, it is not possible to cancel this base disturbance using static state feedback. This complicates the motion planning and control issue further (Nakamura and Mukherjee 1991).

The dynamic coupling between space vehicle and manipulators has been a subject of intense investigation since the Space Shuttle RMS went into service in 1982. Due to dynamic coupling, the resulting motion at the shuttle base caused the end-effector to miss its target. This type of problem can be particularly acute during satellite rendezvous in which errors of even a few centimeters could result in a failed capture attempt or even damage to the satellite. Also vehicle attitude disturbance assumes prime importance because any disorientation would affect the communication link of the satellite with the control station. One of the key issues in space robotics is using arms to contact worksite elements safely, quickly, and accurately without accidentally contacting unintended objects or imparting excessive forces beyond those needed for the task. For this purpose trajectory planning assumes importance. A well planned trajectory, taking care of singularities of manipulator arm, is essential for efficient and smooth controlled motion of arm tips.

Control of space robot has been studied by many authors but control studies on multi arm space robot are only few. Dubowsky and Papadopoulos (1993a, 1993b) discussed concepts of virtual Manipulator (VM) model with an application to workspace analysis, path planning using Enhanced Disturbance Map (EDM) as well as effects of dynamic singularities on workspace of free flying manipulator. Moosavian and Papadopoulos (1998) proved the advantage of Direct Path Method over Barycentric vector approach while developing kinematic modeling of rigid multi arm space robots. Papadopoulos and Moosavian (1994) compared by simulation study, the performance of Euler angle and Euler parameter base control law to that of a transposed Jacobian algorithm and showed that the latter gives reasonably good performance with reduced computational burden. Huang, Xu, and Liang (2005) developed a space robot system consisting of two arms, with one arm (mission arm) for accomplishing the capture mission, and the other one (balance arm) compensating for the disturbance of the base. Marchesi

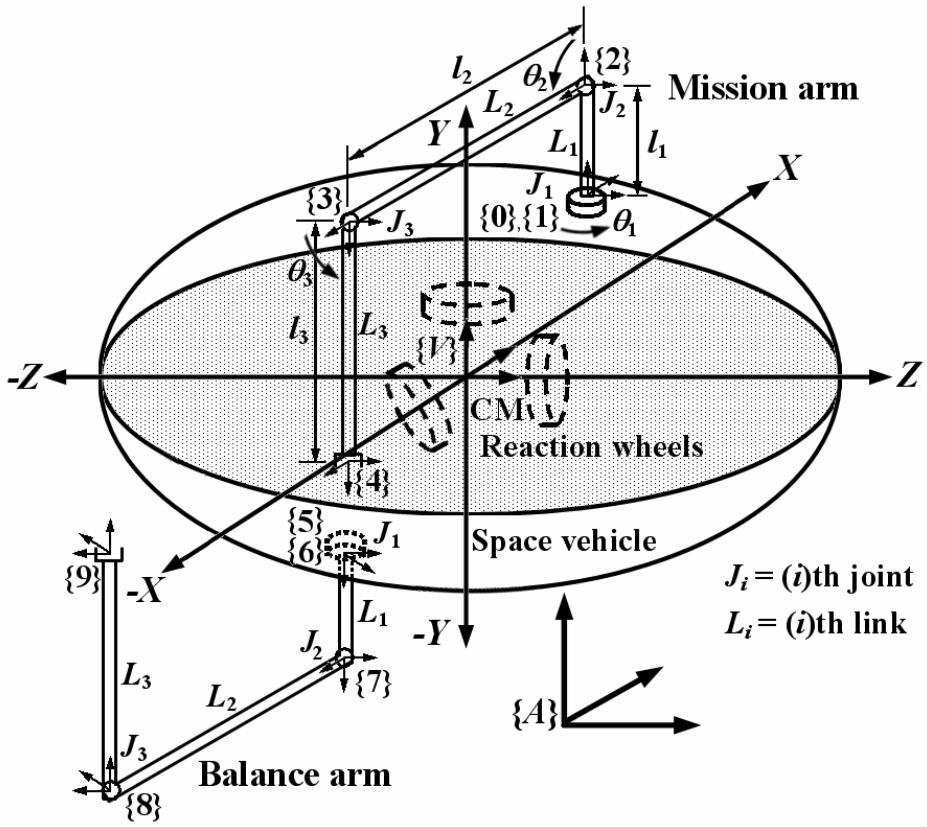

Figure 1: Schematic Diagram of Three DOF Dual Arm Space Robot

and Angrolli (1997) focused on control strategy for a free-flying space manipulator and described the methods used to solve the inverse kinematic problem of a non-redundant robotic arm mounted on a free floating spacecraft for minimal disturbance of spacecraft attitude. Yokokohji, Toyoshima, and Yoshikawa (1993) proposed an efficient computation algorithm for the trajectory control of multi arm free-flying space robot using the generalized Jacobian matrix technique. Chen and Tang (2006) presented the optimal non-holonomic motion planning of free-floating space robot system with dual arms.

Based on the insights developed from bond graph modeling, Ghosh (1990) developed a robust overwhelming controller for the robotic manipulator, which does not require the knowledge of the robot parameters and the payload. Pathak, Kumar, Mukherjee, and Dasgupta (2008) presented a scheme for robust trajectory control of free-floating space robots.

This work presents a strategy for trajectory control of mission arm with small attitude disturbance of vehicle. Trajectory control of mission arm is achieved by using robust overwhelming controller (Ghosh 1990; Pathak, Kumar, Mukherjee, and Dasgupta 2008; Mukherjee, Karmakar, and Samantray 2006). Due to mission arm tip motion, vehicle attitude gets disturbed. A control law is proposed for joint control of balance arm such that when it works with trajectory control of mission arm small vehicle attitude disturbance is obtained. It is assumed that the space vehicle is equipped with three small reaction wheels. A numerical example of free-floating space vehicle carrying two manipulators, each of having three links is presented to demonstrate the efficacy of the proposed control strategy. The complete dynamics is modeled using bond graphs (Karnopp, Margolis, and Rosenberg 2006; Mukherjee, Karmakar, and Samantray 2006; Breedveld and Dauphin-Tanguy 1992). For the purpose of modeling and simulation, the bond graph package SYMBOLS Shakti (Users Manual) has been used.

2. MODELING OF THREE DOF DUAL ARM SPACE ROBOT

To illustrate the control strategy for the space robot, a three DOF free-floating space robot consisting of two serial manipulators each of having three links mounted on a space vehicle is considered and shown in Figure 1.

Joint rotation (θ_i) of manipulator and Euler angle of the base (ϕ, θ, ψ) in 3-2-1 convention are used as generalized coordinates. All joints are assumed to be revolute. The joint between links (i) and (i+1) is numbered as (i+1). In Figure 1, {A} is the absolute frame and {V} is the vehicle frame located at the centre of mass (CM) of the vehicle. The frames {0} and {5} are attached on the vehicle to represent the mission arm and balance arm base location on the vehicle at a position (r_x, r_y, r_z) and (-r_x, -r_y, -r_z) from the origin of frame {V}, respectively. The frames {1} and {6} are attached on the first links of mission arm and balance arm at their bases, respectively. The frames {1} and {6} have relative motion with respect to frames {0} and {5} about Y-axis. Frames {2} and {3} are attached at the

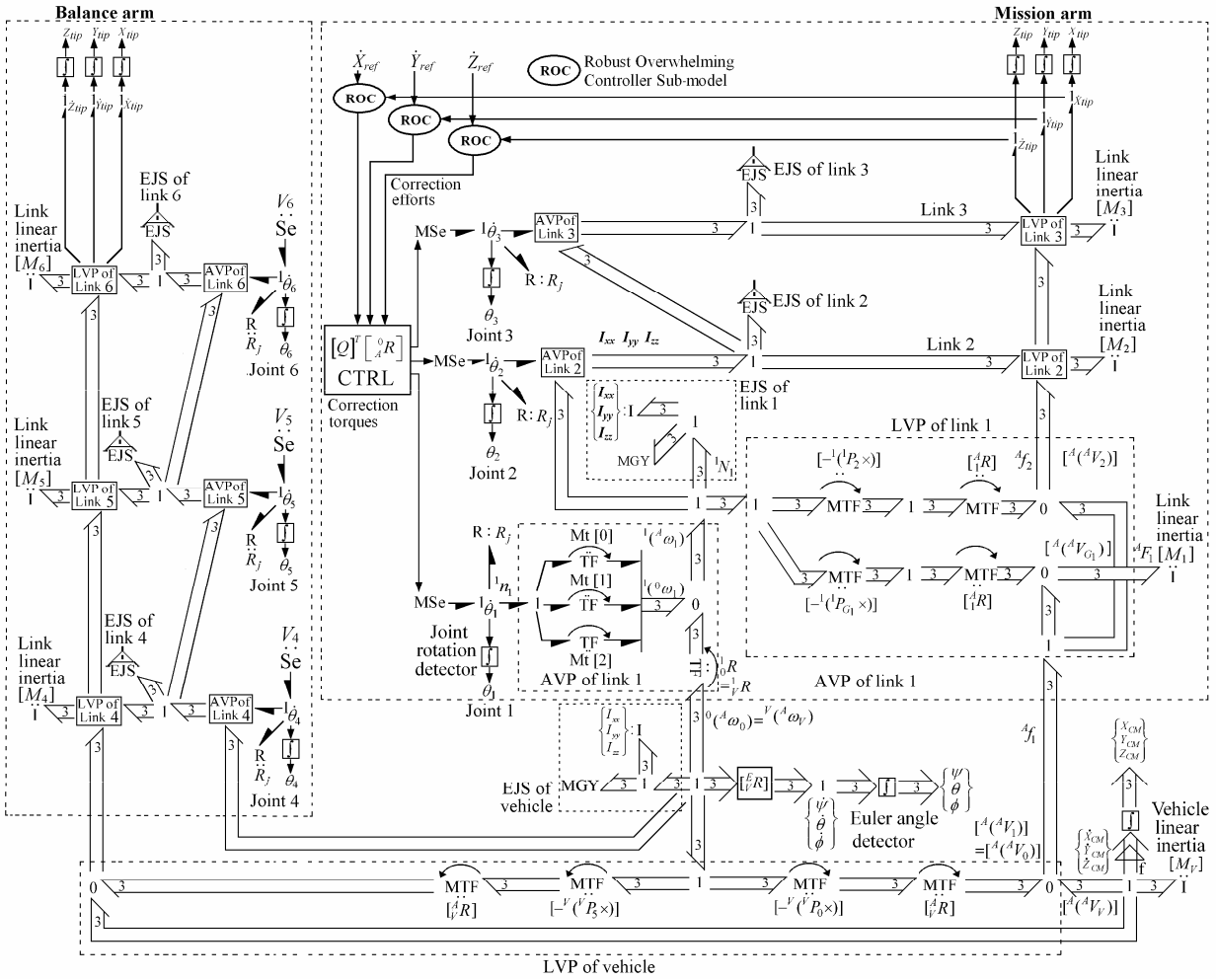

Figure 2: Multi Bond Graph Model of Three DOF Dual Arm Space Robot

base of second and third links of the mission arm whereas frames {7} and {8} are attached at the base of second and third links of the balance arm, respectively. They represent the joint axes for the second and third joints of both the arms and have rotation about their *Z*-axes. The moments of inertia are defined about the body-fixed principal coordinate system. It is assumed that all the links are to be rigid and the specified task space trajectory is within the reachable workspace of the manipulators for simplicity. The frames {4} and {9} represent the tips of mission and balance arm, respectively.

The angular relative velocities of links of the mission arm are defined as,

$$
\begin{aligned}
{}^{1}\omega_1 &= [0 \quad \dot{\theta}_1 \quad 0]^T \\
{}^{2}\omega_2 &= [0 \quad 0 \quad \dot{\theta}_2]^T \\
{}^{3}\omega_3 &= [0 \quad 0 \quad \dot{\theta}_3]^T
\end{aligned} \tag{1}
$$

Here $\dot{\theta}_1$, $\dot{\theta}_2$ and $\dot{\theta}_3$ are the joint velocities of first, second and third joints of the mission arm, respectively.

Modeling of dual arm space robot involves modeling of the linear and angular dynamics of the manipulators as well as the space vehicle on which they are mounted. The complete bond graph model of three DOF dual arm space robot is created and shown in Figure 2. Various sub-models required for drawing bond graph model are briefly presented here.

2.1. Kinematic Relations

A signal structure has been made for transforming the vehicle angular velocity to Euler angle rates using the relation,

$$
\begin{bmatrix} \dot{\psi} \\ \dot{\theta} \\ \dot{\phi} \end{bmatrix} = \begin{bmatrix} 1 & t\theta s\psi & t\theta c\psi \\ 0 & c\psi & -s\psi \\ 0 & s\psi / c\theta & c\psi / c\theta \end{bmatrix} \begin{bmatrix} \omega_x \\ \omega_y \\ \omega_z \end{bmatrix} \tag{2}
$$

where $\dot{\psi}$, $\dot{\theta}$ and $\dot{\phi}$ are the Euler angle rates; ω_x, ω_y and ω_z are the vehicle angular velocities. Also $t\theta = \tan\theta$, $c\theta = \cos\theta$, $c\psi = \cos\psi$ and $s\psi = \sin\psi$. The angular velocity of (i+1)th link with respect to the absolute frame {A}, ${}^{i+1}({}^{A}\omega_{i+1})$ can be computed recursively using the following relation (Craig, 1986),

$$
{}^{i+1}({}^{A}\omega_{i+1}) = {}^{i+1}_{i}R \; {}^{i}({}^{A}\omega_i) + \dot{\theta}_{i+1} \; {}^{i+1}\hat{U}_{i+1} \tag{3}
$$

where ${}^{i+1}_{i}R$ is the rotation matrix of direction cosines relating frame {i} with respect to frame {i+1}, ${}^{i}({}^{A}\omega_i)$ is the angular velocity of (i)th link with respect to the absolute frame {A}, $\dot{\theta}_{i+1}$ is the velocity of (i+1)th joint and ${}^{i+1}\hat{U}_{i+1}$ is a unit vector representing the direction of the joint axis. This computation is implemented through angular velocity propagation (AVP) sub-model of link as shown in Figure 2. This sub-model takes the angular velocity of previous link and the joint velocity between the previous and current link as input and the angular velocity of the current link is given out after calculation. The joint velocity $\dot{\theta}_{i+1}$ is relative between two adjacent links, can be about any one of the axes of the joint coordinate frame. Based on the axis of the joint rotation, one of the transfer moduli (Mt[0], Mt[1] or Mt[2]) connected to the joint velocity junction will be unity, and the remaining will be zero. This is decided by the vector ${}^{i+1}\hat{U}_{i+1}$.

The relation for linear velocity of the tip of the link can be computed as,

$$ {}^{A}({}^{A}V_{i+1}) = {}^{A}({}^{A}V_i) + {}^{A}_{i}R[{}^{i}({}^{A}\omega_i) \times {}^{i}({}^{i}P_{i-1})] \quad (4) $$

where ${}^{i}({}^{i}P_{i+1}) = \begin{bmatrix} 0 \\ l_i \\ 0 \end{bmatrix}$, $[{}^{i}({}^{i}P_{i+1}\times)] = \begin{bmatrix} 0 & 0 & l_i \\ 0 & 0 & 0 \\ -l_i & 0 & 0 \end{bmatrix}$, and

l_i = length of (i)th link.

The linear velocity of the CM of the link can be obtained by using ${}^{i}({}^{i}P_{Gi}) = [0 \quad l_{Gi} \quad 0]^T$ in place of ${}^{i}({}^{i}P_{i+1})$ in Eq. (4). The bond graph sub-model for linear velocity propagation (LVP) of link is created and is shown in Figure 2. This sub-model takes the angular velocity of current link and tip velocity of previous link as input and gives velocity of CM of current link and tip velocity of current link as output. The CM velocities of the space vehicle and links of the manipulators are obtained from the linear inertia of the space vehicle and links, respectively. In Figure 2, $1_{\dot{\theta}_i}$ junctions represent the joint relative velocities and the integrator sub-models used as displacement detectors.

2.2. Euler Junction Structure

A rigid body has translation and angular motion. Thus its dynamics has two parts. The translation dynamics is modeled using Euler's first law and the angular dynamics using the Euler's second law. In order to model the Euler's equations, the gyrator loop commonly known as an Euler Junction Structure (EJS) is used and a sub-model EJS is created to represent the rotational dynamics of the space vehicle and that of the links. The following Euler equations are used to create the sub-model EJS,

$$ N_x = I_{XX}\dot{\omega}_x + (I_{ZZ} - I_{YY})\omega_y\omega_z \quad (5) $$

$$ N_y = I_{YY}\dot{\omega}_y + (I_{XX} - I_{ZZ})\omega_z\omega_x \quad (6) $$

$$ N_z = I_{ZZ}\dot{\omega}_z + (I_{YY} - I_{XX})\omega_x\omega_y \quad (7) $$

here N_x, N_y and N_z represent the moments acting on the vehicle expressed in vehicle frame in X, Y, and Z direction, respectively. I_{XX}, I_{YY} and I_{ZZ} are the moment of inertia of the rigid body about X, Y and Z directions, respectively. The created sub-model EJS is shown in Figure 2.

3. CONTROLLER DESIGN OF SPACE ROBOT

3.1. Trajectory Control of Mission Arm

For the mission arm tip trajectory control, robust overwhelming controller (ROC) presented elsewhere, is used. The bond graph sub-model for ROC is shown in Figure 3. A reference flow input for plant is supplied to sub-model ROC from main bond graph which is shown in Figure 2. This sub-model is also provided with mission arm tip velocity as input from main bond graph

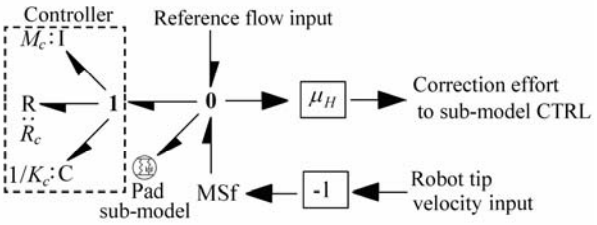

Figure 3: Robust Overwhelming Controller (ROC) Sub-model

and it gives correction efforts as output to sub-model CTRL. In Figure 3, pad sub-model is used to avoid differential causality. Pads are lumped flexibilities with high values of stiffness and damping. Three ROC sub-models (one for each X, Y and Z direction) are used to control the space robot as shown in Figure 2. A signal structure CTRL can be created using forward kinematic relations to convert correction efforts from ROC into correction torques to be supplied to different joints of the mission arm. For creation of this signal structure CTRL, the tip velocity of the mission arm with respect to its base frame {0} expressed in absolute frame {A} can be evaluated as,

$$ {}^{A}({}^{0}V_4) = {}^{A}_{0}R\ {}^{0}({}^{0}V_4) \quad (8) $$

here, ${}^{k}({}^{j}V_i)$ denotes the velocity of the origin of {i}th frame as observed from {j}th frame and expressed in {k}th frame, ${}^{A}_{0}R$ represents the orientation of a frame {0} with respect to a frame {A}. The term ${}^{0}({}^{0}V_4)$ in Eq. (8) can be derived as,

$$ {}^{0}({}^{0}V_4) = \begin{bmatrix} (s_1s_2l_2 + s_1s_{23}l_3) & -(c_1c_2l_2 + c_1c_{23}l_3) & -c_1c_{23}l_3 \\ 0 & -(s_2l_2 + s_{23}l_3) & -s_{23}l_3 \\ (c_1s_2l_2 + c_1s_{23}l_3) & (s_1c_2l_2 + s_1c_{23}l_3) & s_1c_{23}l_3) \end{bmatrix} \begin{Bmatrix} \dot{\theta}_1 \\ \dot{\theta}_2 \\ \dot{\theta}_3 \end{Bmatrix} \quad (9) $$

where $c_i = \cos\theta_i$, $s_i = \sin\theta_i$, $c_{ij} = \cos(\theta_i + \theta_j)$ and $s_{ij} = \sin(\theta_i + \theta_j)$. One can write Eq. (9) in a compact form as,

$$^0(^0V_4) = [Q][\dot{\theta}_1 \quad \dot{\theta}_2 \quad \dot{\theta}_3]^T \tag{10}$$

where [*Q*] is the transformation matrix in Eq. (9). The transformation ${}^A_0R$ is computed as ${}^A_0R = {}^A_V R\ {}^V_0R$ where,

$${}^A_V R = \begin{bmatrix} c\phi c\theta & c\phi s\theta s\psi - s\phi c\psi & c\phi s\theta c\psi + s\phi s\psi \\ s\phi c\theta & s\phi s\theta s\psi + c\phi c\psi & s\phi s\theta c\psi - c\phi s\psi \\ -s\theta & c\theta s\psi & c\theta c\psi \end{bmatrix} \tag{11}$$

and ${}^V_0R$ is identity matrix, $c\phi = \cos\phi$, $s\phi = \sin\phi$, $c\psi = \cos\psi$, $s\psi = \sin\psi$, $c\theta = \cos\theta$ and $s\theta = \sin\theta$. Thus Eq. (8) can be written as,

$$^A(^0V_4) = [{}^A_0R][Q][\dot{\theta}_1 \quad \dot{\theta}_2 \quad \dot{\theta}_3]^T \tag{12}$$

Thus, the relationship between joint correction torques and correction efforts from controller can be expressed as,

$$[{}^1\eta_1 \quad {}^2\eta_2 \quad {}^3\eta_3]^T = [Q]^T [{}^0_A R][F_x \quad F_y \quad F_z]^T \tag{13}$$

where ${}^i\eta_i$ is the torques exerted on link (*i*) by link (*i*-1), expressed in terms of frame {*i*}. F_x, F_y and F_z are corrective efforts in *X*, *Y* and *Z* directions, respectively. The created sub-model CTRL for signal structure for conversion of correction efforts to correction torques is shown in Figure 2.

3.2. Attitude Control of Space Vehicle

The proposed control strategy for attitude control of space vehicle can be worked out as,

(i) Assuming that the motions of actuators at first and second joints of mission arm and balance arm are equal and opposite direction to each other. The control law for the actuators at first and second joints of the balance arm can be given as,

$$\tau_{Bj} = K_p(-\theta_{Mj} - \theta_{Bj}) + K_v(-\dot{\theta}_{Mj} - \dot{\theta}_{Bj}) \text{ for } j = 1, 2. \tag{14}$$

here τ_{Bj} is the torque at (*j*)th joint of balance arm; θ_{Mj} is the position of (j)th joint of mission arm; θ_{Bj} is the position of (*j*)th joint of balance arm; $\dot{\theta}_{Mj}$ is the (*j*)th joint angular velocity of mission arm; $\dot{\theta}_{Bj}$ is the (*j*)th joint angular velocity of balance arm; K_p is proportional gain parameter and K_v is derivative gain parameter.

(ii) The control law for the actuator at third joint of balance arm can be written as,

$$\begin{aligned} \tau_{B3} = {} & K_p(\psi_d - \psi_a) + K_v(\dot{\psi}_d - \dot{\psi}_a) \\ & + K_p(\theta_d - \theta_a) + K_v(\dot{\theta}_d - \dot{\theta}_a) \\ & + K_p(\phi_d - \phi_a) + K_v(\dot{\phi}_d - \dot{\phi}_a) \end{aligned} \tag{15}$$

where τ_{B3} is the torque at third joint of balance arm; ψ, θ and ϕ are the Euler angles; $\dot{\psi}$, $\dot{\theta}$ and $\dot{\phi}$ are the Euler angle rates; suffix 'd' stands for 'desired' whereas suffix 'a' stands for 'actual'. This control law has been devised based on the observation that the body attitude is controllable from the joints of the balance arm (Dauphin-Tanguy, Rahmani, and Sueur, 1999).

4. SIMULATION AND RESULTS

To validate the control strategy discussed in Section 2 and 3, a bond graph model as shown in Figure 2 has been simulated. The parameters used for the simulation are given in Appendix A. It is assumed that initially the absolute frame and vehicle frame are coincident. For the simulation, the reference velocity command for mission arm in absolute frame is taken as,

$$\dot{X}_{ref} = R\omega\sin(\omega t) \quad \text{in } X \text{ direction} \tag{16}$$

$$\dot{Y}_{ref} = A\sin(2\omega t) \quad \text{in } Y \text{ direction} \tag{17}$$

$$\dot{Z}_{ref} = R\omega\cos(\omega t) \quad \text{in } Z \text{ direction} \tag{18}$$

where *R* is the radius of the reference circle in *X*-*Z* plane; *A* is the amplitude of velocity in *Y* direction. It is a circular trajectory in *X*-*Z* plane and parabolic

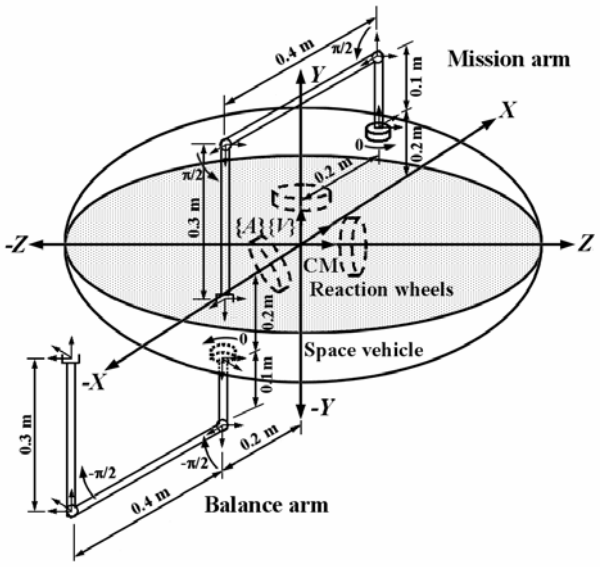

Figure 4: Initial Configuration of Three DOF Dual Arm Space Robot

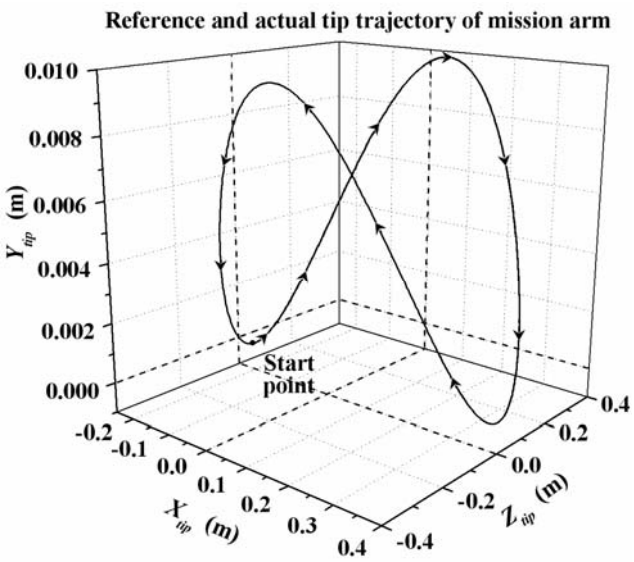

Figure 5: 3-D Plot of Reference and Actual Tip Trajectory of Mission Arm

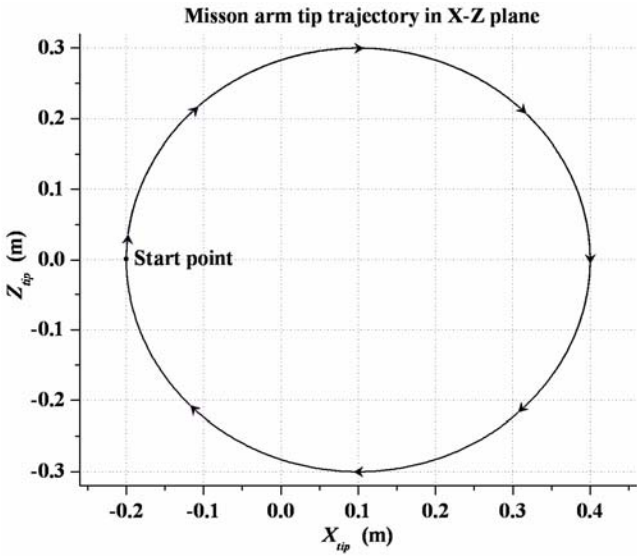

Figure 6: Plot of Reference and Actual Tip Trajectory of Mission Arm in *X-Z* Plane

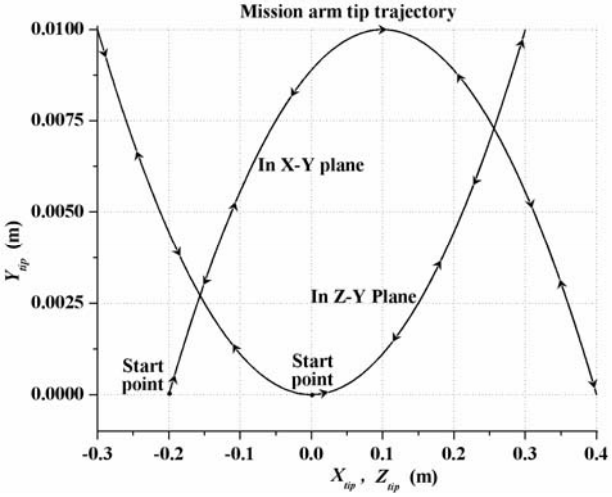

Figure 7: Plot of Reference and Actual Tip Trajectory of Mission Arm in *X-Z* and *Z-Y* Plane

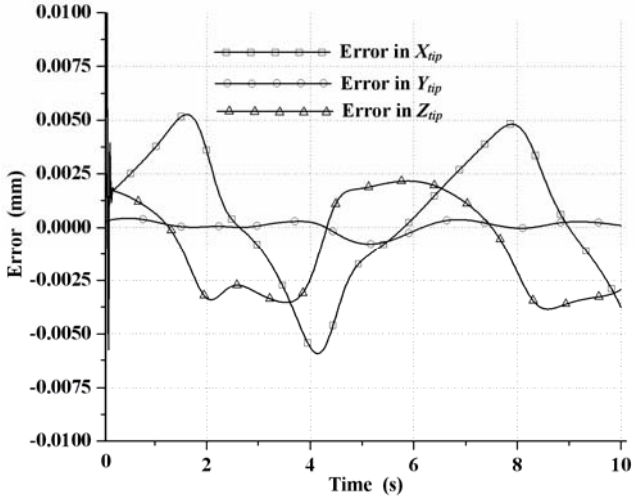

Figure 8: Plot of Mission Arm Tip Position Error versus Time

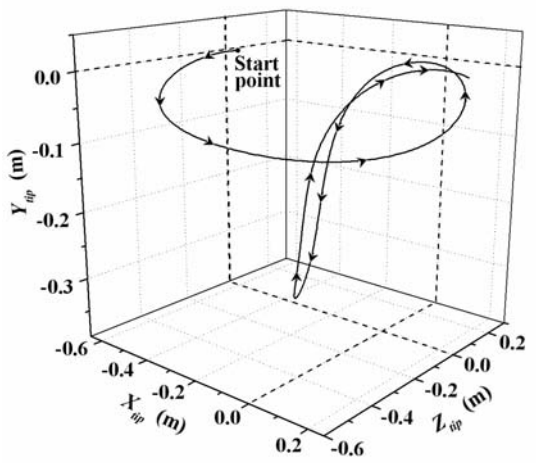

Figure 9: 3-D Plot of Actual Tip Trajectory of Balance Arm

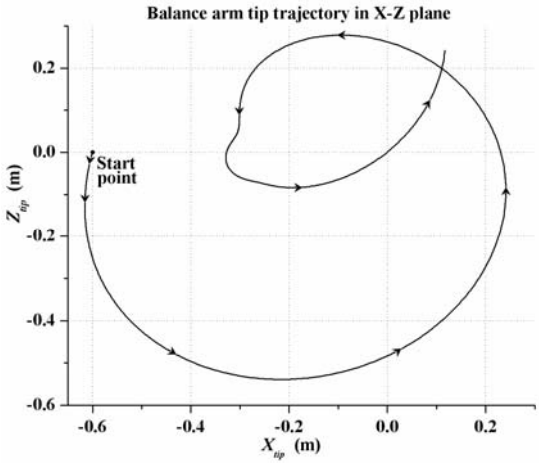

Figure 10: Plot of Actual Tip Trajectory of Balance Arm in *X-Z* Plane

trajectory in *X-Y* plane and *Y-Z* plane. The joint torques for balance arm is given as per control law shown in Eq. 14 and 15. At the beginning of the simulation, the overwhelmer initial position is set to mission arm tip position in order to keep the initial error to be zero.

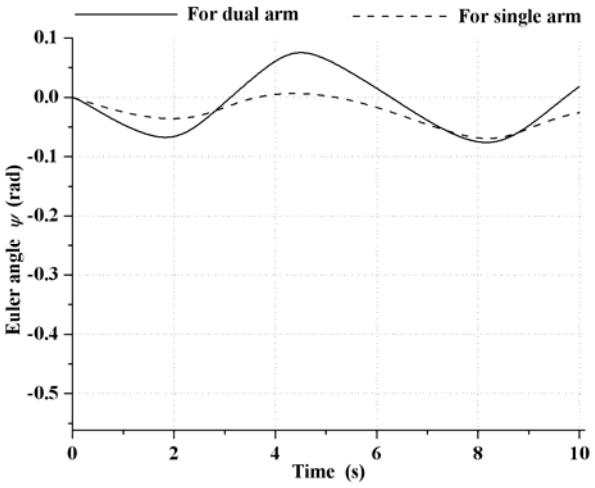

Figure 11: Plot of Variation of Euler Angle ψ for Single and Dual Arm Space Vehicle versus Time

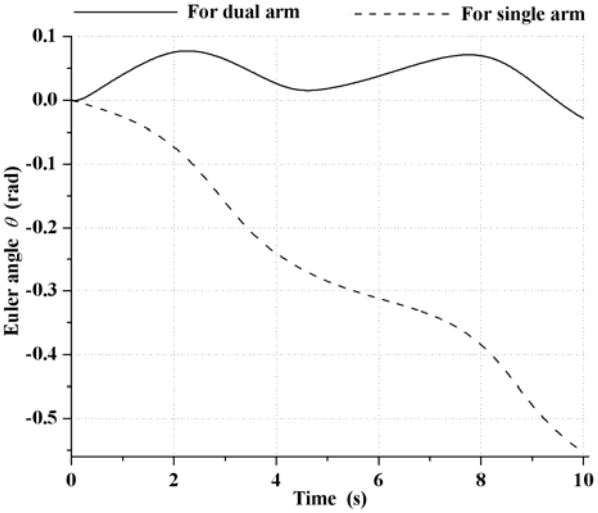

Figure 12: Plot of Variation of Euler Angle θ for Single and Dual Arm Space Vehicle versus Time

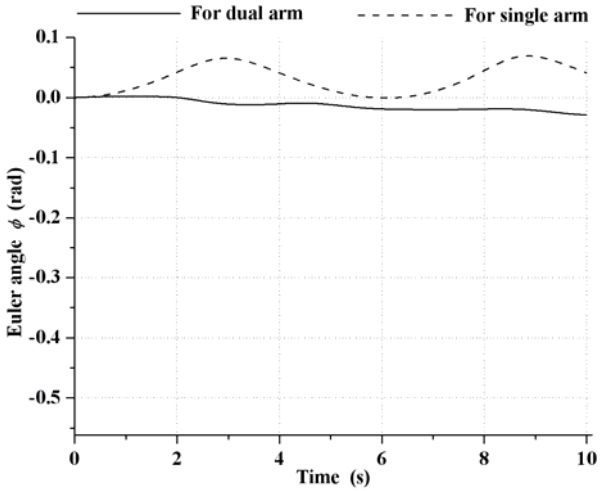

Figure 13: Plot of Variation of Euler Angle ϕ for Single and Dual Arm Space Vehicle versus Time

As the reaction wheels are provided to introduce the redundancy in the system, the input source of voltage to them is kept zero. In this condition, they will only follow the attitude of the vehicle base. However reaction wheels can be actuated by input source of voltage as and when required. The initial configuration of the space robot is shown in Figure 4. The simulation is carried out for 10 seconds.

A three-dimensional plot of reference and actual trajectories of tip of the mission arm are shown in Figure 5. The reference and actual tip trajectories of the mission arm in *X-Z* plane are shown in Figure 6, whereas in Figure 7, the reference and actual tip trajectories of the mission arm in *X-Y* and *Z-Y* planes are shown. Figure 8 shows the plots of error between the reference and actual tip positions with respect to time for mission arm. Here for mission arm, X_{tip} position error varies between -0.0059 to +0.0053 mm, Y_{tip} position error varies between -0.0008 to +0.0004 mm and that of Z_{tip}, it varies between -0.0036 to +0.0021 mm, except the initial phase and it is due to that the tip acquires a velocity from the rest position. From Figure 5 to 8, it is observed that mission arm tip is effectively dragged along the reference trajectory.

Figure 9 shows a three-dimensional plot of the balance arm tip trajectory. The trajectory followed by tip of the balance arm in *X-Z* plane is presented in Figure 10. From Figure 9 and 10, it is seen how the balance arm tip moved while controlling the space vehicle attitude disturbance.

The variations in Euler angles ψ, θ, and ϕ for the space vehicle carrying two arms as well as the space vehicle carrying single arm (mission arm) only with respect to time are shown in Figure 11, 12 and 13, respectively. From these figures, it is observed that for a same set of parameters and reference trajectory that of the dual arm, the space vehicle carrying single arm having a continuous drift in Euler angle θ from 0 to -0.553 radians. The space vehicle carrying two arms, the variation in Euler angle θ is reduced significantly and is between -0.028 to +0.077 radians only. The variation in Euler angle ϕ for single arm space vehicle is 0.0 to +0.065 radians and it is further improved for dual arm space vehicle which varies from 0 to -0.028 radians. However, there is no any improvement in Euler angle ψ but it varies between -0.075 to +0.075 radians for dual arm space vehicle.

5. CONCLUSION

This work contributes a control strategy for small attitude disturbance of space vehicle while mission arm follows the desired trajectory. Here our objective is that the mission arm should follow the desired trajectory but vehicle attitude disturbance should be small. This objective has been achieved with the help of the proposed control laws of balance arm.

ACKNOWLEDGMENTS

We are thankful to Indian Space Research Organization (ISRO) for funding the project vides Grant No. ISRO/RES/3/596/09-10.

APPENDIX A
Parameters used in simulation

Link Parameters	Mass (kg)	Length l_i (m)	Length l_{Gi} (m)	I_{XX} (kg m^2)	I_{YY} (kg m^2)	I_{ZZ} (kg m^2)	Initial Joint angle θ (rad)
For mission arm							
Link 1	6.13	0.1	0.05	0.0300	0.0250	0.0300	0
Link 2	15.69	0.4	0.20	0.2153	0.0126	0.2153	$\pi/2$
Link 3	11.76	0.3	0.15	0.0929	0.0094	0.0929	$\pi/2$
For balance arm							
Link 1	6.13	0.1	0.05	0.0300	0.0250	0.0300	0
Link 2	15.69	0.4	0.2	0.2153	0.0126	0.2153	$-\pi/2$
Link 3	11.76	0.3	0.15	0.0929	0.0094	0.0929	$-\pi/2$
Space vehicle	200.0	-	-	40.000	40.000	40.000	-

Initial Arm Base Position from Vehicle CM		
	Mission Arm	**Balance Arm**
r_x	0.2 m	-0.2 m
r_y	0.2 m	-0.2 m
r_z	0.0 m	0.0 m

Overwhelming Controller Parameters	**Parameter value**
Mass (M_c)	1.0 kg
Stiffnesss (K_c)	1e5 N/m
Rasistance (R_c)	1e3 Ns/m
Feed forward gain (μ_H)	10.0
Attitude Controller Gain Parameters	
Proportional gain of controller (*Kp*)	10
Derivative gain of controller (*Kv*)	5
Reference Trajectory Parameters	
Radius of reference circle (*R*)	0.3 m
Amplitude of velocity in *Y*-direction (*A*)	0.01 m
Angular velocity (ω)	1.0 rad/s
Actuator and reaction wheel Parameters	
Inductance of the armature (I_m)	0.001 H
Resistance of the armature (R_m)	0.2 ohm
Inertia of reaction wheel (I_{RW})	0.5 kg m^2
Bearing resistance for reaction wheel (R_b)	0.02 Nm/rad/s
Pad Parameters	
Stiffness of hard spring (K_h)	2e5 N / m
Stiffness of soft spring (K_s)	1e5 N/m
Damping resistance (R_d)	1e3 Ns/m
Joint Resistance (R_j)	0.1 Nm/rad/s

REFERENCES

Dauphin-Tanguy, G., Rahmani, A., and Sueur, C., 1999. Bond graph Aided Design of Controlled Systems. *Simulation Practice and Theory*, 7(5-6), 493-513.

Dubowsky, S. and Papadopoulos, E., 1993a. The Kinematics, Dynamics, and Control of Free-Flying and Free-Floating Space Robotic Systems. *IEEE Transactions on Robotics and Automation*, 9(5), 531-543.

Dubowsky, S. and Papadopoulos, E., 1993b. Dynamic Singularities in the Control of Free-Floating Space Manipulators. *ASME Journal of Dynamic Systems, Measurement and Control*, 115(1), 44-52.

Huang, P., Xu, Y., and Liang, B., 2005. Dynamic Balance Control of Multi-arm Free-Floating Space Robots. *International Journal of Advanced Robotic Systems*, 2(2), 117-124.

Moosavian, S. A. A. and Papadopoulos, E., 1998. On the Kinematics of Multiple Manipulator Space Free-Flyers and their Computation. *Journal of Robotic Systems*, 15(4), 207-216.

Nakamura, Y. and Mukherjee R., 1991. Non-holonomic Path Planning of Space Robots via a Bidirectional Approach. *IEEE Transactions on Robotics and Automation*, 7(4), 500-514.

Pathak, P. M., Kumar, R. P., Mukherjee, A., and Dasgupta, A., 2008. A Scheme for Robust Trajectory Control of Space Robots. *Simulation Modeling Practice and Theory*, 16(9), 1337-1349.

Yokokohji, Y., Toyoshima, T., and Yoshikawa, T., 1993. Efficient Computational Algorithms for Trajectory Control of Free-Flying Space Robots with Multiple Arms. *IEEE Transactions on Robotics and Automation*, 9(5), 571-579.

Chen, L. and Tang, X., 2006. Optimal Motion Planning of Attitude Control for Space Robot System with Dual-arms, *Proceedings of 6th World Congress on Intelligent Control and Automation*, pp. 8858-8861. June 21-23, Dalian, China.

Marchesi, M. and Angrilli, F., 1997. Control Strategy for a Free-flying Space Manipulator. *Proceedings of 8th International Conference on Advanced Robotics*, pp. 665-670. July 7-9, Monterey, CA.

Papadopoulos, E. and Moosavian, S. A. A., 1994. Dynamics and Control of Multi-arm Space Robots during Chase and Capture Operations. *Proceedings of the International Conference on Intelligent Robots and Systems*, pp. 1554-1561. September 12-16, Munich, Germany.

Breedveld, P. C. and Dauphin-Tanguy, G., 1992. *Bond Graphs for Engineers*, Amsterdam North-Holland, Elsevier.

Craig, J. J., 1986. *Introduction to Robotics–Mechanics and Control*, Addison-Wesley Publishing Co.

Karnopp, D. C., Margolis, D. L., and Rosenberg, R. C., 2006. *System Dynamics: Modeling and Simulation of Mechatronics Systems*, New Jersey, John Wiley and Sons Inc.

Mukherjee, A., Karmarkar, R., and Samantray, A. K., 2006. *Bond graph in Modeling, Simulation and Fault Identification*, India, I.K. International Publishing House Pvt. Ltd.

Ghosh, A. K., 1990. *Dynamics and robust control of robotic system: a bond graph approach*. Thesis (PhD). Department of Mechanical Engineering, Indian Institute of Technology, Kharagpur, India.

Users Manual of SYMBOLS Shakti, 2006. High-Tech Consultants, S.T.E.P., Indian Institute of Technology, Kharagpur. http://www.htcinfo.com/

AUTHORS BIOGRAPHY

Haresh Patolia received the B. E. degree in 1991and M. E. degree in 2001, both in Mechanical Engineering from B. V. Mahavidyalaya, V. V. Nagar, India. He joined the Department of Mechanical Engineering at B. V. Mahavidyalaya, V. V. Nagar, India in 1994. Currently he is a Ph. D. candidate at the Department of Mechanical and Industrial Engineering, Indian Institute of Technology, Roorkee, India.

P. M. Pathak received the B. Tech. degree in 1988 from R. E. College, Calicut, India and M. Tech. degree in 1998 from IIT, Kanpur, India both in Mechanical Engineering. He received Ph. D. degree in 2004 from IIT, Kharagpur, India. He is an Assistant Professor at the Department of Mechanical and Industrial Engineering, Indian Institute of Technology, Roorkee, India. His areas of interest are space robotics, walking robots, dynamics and control.

S. C. Jain received the B. Sc. Engg. degree in 1969 from AMU, Aligarh, India and M. E. degree in 1971 from University of Roorkee, India, both in Mechanical Engineering. He received Ph. D. degree in 1985 from University of Roorkee, India. He is a Vice-Chancellor at Mangalayatan University, Aligarth, India. His areas of interest are tribology, vibration and noise control, CAD, and robotics.